Analysis of dilepton production in Au + Au collisions at $\sqrt{s_{NN}} = 200$ GeV within the parton-hadron-string dynamics transport approach

O. Linnyk* and W. Cassing
Institut für Theoretische Physik, Universität Giessen, D-35392 Giessen, Germany

J. Manninen and E. L. Bratkovskaya
Institut für Theoretische Physik, Johann Wolfgang Goethe University, D-60438 Frankfurt am Main, Germany and Frankfurt Institute for Advanced Studies, D-60438 Frankfurt am Main, Germany

C. M. Ko
Cyclotron Institute and Department of Physics and Astronomy, Texas A&M University, College Station, Texas 77843-3366, USA
(Received 12 November 2011; published 29 February 2012)

We address dilepton production in Au + Au collisions at $\sqrt{s_{NN}} = 200$ GeV by employing the parton-hadron-string dynamics (PHSD) off-shell transport approach. Within the PHSD, one goes beyond the quasiparticle approximation by solving generalized transport equations on the basis of the off-shell Kadanoff-Baym equations for the Green's functions in the phase-space representation. The approach consistently describes the full evolution of a relativistic heavy-ion collision, from the initial hard scatterings and string formation, through the dynamical deconfinement phase transition to the quark-gluon plasma (QGP) as well as hadronization, to the subsequent interactions in the hadronic phase. With partons described in the PHSD by the dynamical quasiparticle model (DQPM)—matched to reproduce lattice QCD results in thermodynamic equilibrium—we calculate, in particular, the dilepton radiation from partonic interactions through the reactions $q\bar{q} \to \gamma^*$, $q\bar{q} \to \gamma^* + g$, and $qg \to \gamma^* q$ ($\bar{q}g \to \gamma^* \bar{q}$) in the early stage of relativistic heavy-ion collisions. By comparing our results to the data from the PHENIX Collaboration, we study the relative importance of different dilepton production mechanisms and point out the regions in phase space where partonic channels are dominant. Furthermore, explicit predictions are presented for dileptons within the acceptance of the STAR detector system and compared to the preliminary data.

DOI: 10.1103/PhysRevC.85.024910 PACS number(s): 25.75.Cj, 25.75.Nq, 24.85.+p

I. INTRODUCTION

The nature of confinement and the phase transition from a partonic system of quarks, antiquarks, and gluons—the so-called quark-gluon plasma (QGP)—to interacting hadrons, as occurs in relativistic nucleus-nucleus collisions, is a central topic of modern high-energy physics. Already some decades ago dileptons were suggested as useful probes of the properties of the QGP [1–5]. Since dileptons are emitted over the entire history of the heavy-ion collision—from the initial nucleon-nucleon collisions, through the hot and dense (partonic) phase, to the hadron decays after freeze-out—microscopic transport models have to be applied to disentangle the various sources that contribute to the final dilepton spectra seen in experiments.

In the present work, we study dilepton production in Au + Au collisions at $\sqrt{s_{NN}} = 200$ GeV within the parton-hadron-string dynamics (PHSD) off-shell transport approach by including the collisional broadening of vector mesons, microscopic secondary multiple-meson channels, and the radiation from the strongly interacting QGP (sQGP) through the interactions of dynamical quasiparticles having broad spectral functions in line with the degrees of freedom propagated in the transport approach.

The PHENIX Collaboration has presented dilepton data from pp and Au + Au collisions at the Relativistic Heavy Ion Collider (RHIC) energy of $\sqrt{s_{NN}} = 200$ GeV [6–8], which show a large enhancement relative to the scaled pp collisions in the invariant mass regime from 0.15 to 0.6 GeV/c^2. The question that we aim to investigate in this work is whether this excess can be attributed to the gluon Compton scattering or other partonic interaction processes, which due to the two-particle finite state contribute at low masses as well.

Moreover, if a realistic partial loss of the D- and $\bar{D}$-meson correlations due to their rescattering is taken into account, one has to conclude from the data of the PHENIX Collaboration that there exists another domain of invariant masses, in which the measured dilepton yield in Au + Au collisions is underestimated by the scaled yield from the $p + p$ collisions, i.e., at masses from 1 to 4 GeV/c^2 [9,10]. The microscopic calculations within the parton-hadron transport approach here will answer if this discrepancy can be accounted for by the partonic sources of dileptons.

In Ref. [11] we have recently presented results from the PHSD for the dilepton spectrum produced in In + In collisions at 158 A GeV and compared them to the NA60 data [12,13]. We recall that by employing the hadron-string dynamics (HSD) transport approach, which does not include explicit partonic contributions to low-mass dilepton production in relativistic heavy-ion collisions, it was shown in Ref. [14] that the NA60 data for the invariant mass spectra of $\mu^+\mu^-$ pairs from In + In collisions at 158 A GeV indicated an in-medium modification of the ρ meson according to the "melting" scenario [12]. The more recent PHSD calculations in Ref. [11], which

*Olena.Linnyk@theo.physik.uni-giessen.de

took into account the phase transition to and the radiation from the partonic phase, confirmed the HSD results that the spectrum at invariant masses in the vicinity of the ρ peak was better reproduced by the ρ-meson yield if a broadening of its spectral function in the medium was assumed. On the other hand, the spectrum at $M > 1$ GeV was shown to be dominated by partonic sources. Moreover, the inclusion of the partonic dilepton sources made it possible to reproduce in the PHSD the effective temperature or the inverse slope parameter of the transverse momentum spectrum of dileptons in the intermediate-mass region. Furthermore, for dileptons of low masses ($M < 0.6$ GeV), a sizable contribution from partonic processes—particularly the quark annihilation with gluon bremsstrahlung in the final state—was found, and this provides another possible window for probing the properties of the sQGP.

In the present work, our previous findings will be reexamined by comparison to the dilepton measurements at RHIC energies. Previous HSD results for e^+e^- pairs in Au + Au collisions in comparison to the data from the PHENIX Collaboration [7,8] were presented in Ref. [14]. Whereas the total yield is quite well described in the low-mass region from the pion Dalitz decay as well as around the ω, ϕ, and J/Ψ masses, the HSD clearly underestimates the measured spectra in the regime from 0.2 to 0.6 GeV by approximately a factor of 5 for central Au + Au collisions. After including the in-medium modification of vector mesons, we obtain a total spectrum that is only slightly enhanced compared to the "free" scenario of using the vector-meson properties in the vacuum (see Fig. 6 of Ref. [14]). The low-mass dilepton spectra from Au + Au collisions obtained by the PHENIX Collaboration at RHIC are thus clearly underestimated in the invariant mass region of 0.2 to 0.6 GeV in the "collisional broadening" scenario as well as in the "dropping mass + collisional broadening" model. We mention that the HSD results for the hadronic production of low-mass dileptons are very close to those calculated by van Hees and Rapp as well as by Dusling and Zahed [15] (cf. the comparisons in Refs. [8] and [16]).

At higher masses, from 1 to 4 GeV, the dominant hadronic sources of lepton pairs are from the semileptonic decays of correlated D mesons and the dilepton decays of charmonia. In estimating this contribution, the experimental information from Ref. [10] was used to determine the yields of charmed hadrons. Additionally, the effect of D-meson rescattering in the hadronic matter was included in the HSD transport approach [17,18] to estimate the probability of surviving correlated semileptonic charm decays in heavy-ion collisions. The resulting dilepton yield between the ϕ and J/Ψ peaks—after including the semileptonic decays of correlated Dmesons in the HSD—was found to underestimate the PHENIX data by approximately a factor of 2 [10].

Another open question to be answered by the microscopic transport calculations is the determination of "windows" in phase space for observing dileptons from the quark-gluon plasma that possibly overshine the hadronic sources. It was originally suggested that a substantial thermal yield from the deconfined phase might be seen in the invariant mass region between the ϕ and J/Ψ peaks [2], while the spectrum at lower masses was dominated by meson decays. On the other hand, the calculations in Refs. [11,19], and [20] pointed to a possible second region of phase space for the observation of the thermal QGP source at masses $\approx$0.3–0.6 GeV. In order to clarify whether these dileptons of masses 0.3–0.6 GeV can be observed among the background of dileptons from hadronic decays, a study within a transport approach that incorporates dilepton production from the (nonequilibrium) partonic phase, hadronic decays, and the microscopic secondary hadronic interactions—including the "4π" channels—thus appears appropriate.

The PHSD [21,22] transport approach, which incorporates the relevant off-shell dynamics of vector mesons and the explicit partonic phase in the early hot and dense reaction region, as well as the dynamics of hadronization, allows for a microscopic study of various dilepton production channels in nonequilibrium matter. The PHSD off-shell transport approach is particularly suitable for investigating the enhanced production of lepton pairs in the invariant mass range $0.3 \leqslant M \leqslant 0.7\ \mathrm{GeV}/c^2$ that is seen in experiments, since it incorporates various scenarios for the modification of vector mesons in a hot and dense medium. In the present work, we calculate the spectra of dileptons produced in the course of Au + Au collisions at $\sqrt{s_{NN}} = 200$ GeV from the partonic and hadronic sources by including the partonic channels and the multiple-meson channels besides the usual hadron decay channels. By consistently treating in the same microscopic transport framework both partonic and hadronic phases of the colliding system, we are aiming to determine the relative importance of different dilepton production mechanisms and to point out the regions in phase space where partonic channels are dominant.

The paper is organized as follows. In Sec. II, we give a brief description of the PHSD approach as well as the hadronic and partonic sources of dilepton production incorporated in the PHSD. We then compare in Sec. III results from our calculations to the available experimental data for Au + Au collisions at top RHIC energy. Finally, our conclusions are presented in Sec. IV.

II. THE PHSD TRANSPORT APPROACH

The PHSD [21,22] is an off-shell transport model that consistently describes the full evolution of a relativistic heavy-ion collision, from the initial hard scatterings and string formation, through the dynamical deconfinement phase transition to the quark-gluon plasma as well as hadronization, to the subsequent interactions in the hadronic phase. In the hadronic sector, the PHSD is equivalent to the HSD transport approach [23–25] that has been used for the description of pA and AA collisions from SIS to RHIC energies and has lead to a fair reproduction of measured hadron abundances, rapidity distributions, and transverse momentum spectra. In particular, as in the HSD, the PHSD incorporates off-shell dynamics for vector mesons [26] and a set of vector-meson spectral functions [27] that covers possible scenarios for their in-medium modifications. The transition from the partonic to hadronic degrees of freedom is described by covariant transition rates for the fusion of quark-antiquark pairs to

mesonic resonances or three quarks (antiquarks) to baryonic states, i.e., the dynamical hadronization [28]. Note that due to the off-shell nature of both partons and hadrons, the hadronization process obeys all conservation laws (i.e., four-momentum conservation and flavor current conservation) in each event, the detailed balance relations, and the increase in the total entropy S. The transport theoretical description of quarks and gluons in the PHSD is based on a dynamical quasiparticle model (DQPM) for partons that is matched to reproduce the lattice QCD (lQCD) results for a quark-gluon plasma in thermodynamic equilibrium. The DQPM provides the mean fields for gluons and quarks and their effective two-body interactions in the PHSD. For details about the DQPM model and the off-shell transport we refer the reader to Ref. [29]. We stress that a nonvanishing width γ in the partonic spectral functions is the main difference between the DQPM and conventional quasiparticle models [30]. Its influence on the collision dynamics is essentially seen in the correlation functions; e.g., in the stationary limit, the correlation involving the off-diagonal elements of the energy-momentum tensor T^{kl} defines the shear viscosity η of the medium [31]. Here a sizable width is mandatory to obtain a small ratio of the shear viscosity to entropy density η/s, which results in a roughly hydrodynamical evolution of the partonic system in PHSD [28]. The finite width leads to two-particle correlations, which are taken into account by means of the *generalized* off-shell transport equations [26], which go beyond the mean-field or Boltzmann approximation [29,32].

A. Partonic sources of dileptons in PHSD

In the scope of the one- and two-particle interactions, dilepton radiation by the constituents of the strongly interacting QGP proceeds via following elementary processes: the basic Born $q + \bar{q}$ annihilation mechanism, gluon Compton scattering ($q + g \to \gamma^* + q$ and $\bar{q} + g \to \gamma^* + \bar{q}$), and quark and antiquark annihilation with the gluon bremsstrahlung in the final state ($q + \bar{q} \to g + \gamma^*$). In the on-shell approximation, one would use perturbative QCD cross sections for the processes listed above. However, in the strongly interacting QGP the gluon and quark propagators differ significantly from the noninteracting propagators. Accordingly, we have calculated in Refs. [33] and [34] the off-shell cross sections for dilepton production in the partonic channels by off-shell partons, using the phenomenological parametrizations (from the DQPM) for the quark and gluon propagators and their interaction strengths.

In Refs. [33] and [34] it was shown that the finite quark and gluon masses modify the magnitude as well as the M and p_T dependence of the cross sections of the above-mentioned processes compared to the perturbative results for massless partons (cf. Figs. 3 and 4 of Ref. [34]). The modifications are large at lower M^2 and at the edges of the phase space. It was shown that the most prominent effect of the quark masses on the dimuon production cross sections in the Born mechanism ($q + \bar{q} \to \gamma^*$) was a sharp threshold value for the invariant mass of the dilepton pair $M_{\min} = m_1 + m_2$. On the other hand, the finite masses of the quark and antiquark produce additional higher-twist corrections to the cross section, which decrease with increasing M^2, so that the off-shell cross sections approach the leading twist—on shell—result in the limit of high dilepton masses. In Fig. 4 of Ref. [34], an analogous comparison for the $2 \to 2$ process $q + \bar{q} \to \gamma^* + g$ was shown by plotting the off-shell (i.e., with finite masses for the quarks and gluons) cross section for the quark annihilation with gluon bremsstrahlung in the final state of various values of the quark and gluon off-shellness (masses) and the corresponding on-shell result. As found in Ref. [34], the maximum pair mass shifts to a lower value as a result of producing a massive gluon in the final state. For the rest of the M values, the effect of the quark and gluon masses is about 50%. For $m_{q/g} \to 0$, the cross section approaches the leading twist perturbative QCD result.

The question of the effect of a finite parton width—which parametrizes their interaction rate and correlation as well as multiple scattering—on dilepton rates in heavy-ion collisions has been addressed in Ref. [34] by convoluting the off-shell cross sections with phenomenological spectral functions $A(m_q)$ and $A(m_g)$ for the quarks and gluons in the quark-gluon plasma, respectively, and with parton distributions in a heavy-ion collision. The finite width of the quasiparticles was found to have a sizable effect on the dilepton production rates. In particular, the threshold of the Drell-Yan contribution was "washed out." Also, the shape and magnitude of the $2 \to 2$ processes ($q + \bar{q} \to g + \gamma^*$ and $q + g \to q + \gamma^*$) were modified. It was further observed that the contribution of the gluon Compton process $q + g \to q + \gamma^*$ to the rates was small compared to that of $q + \bar{q}$ annihilations.

In Ref. [11], we have implemented the cross sections obtained in Refs. [33] and [34] into the PHSD transport approach in the following way: Whenever the quark-antiquark, quark-gluon and antiquark-gluon collisions occur in the course of the Monte-Carlo simulation of the partonic phase in the PHSD, a dilepton pair can be produced according to the off-shell cross sections [34], which depend, in addition to the virtualities of the partons involved, on the energy density in the local cell where the collision takes place. The local energy density governs the widths of the quark and gluon spectral functions as well as the strong coupling, in line with the DQPM.

B. Hadronic sources of dileptons in PHSD

In the hadronic sector, the PHSD is equivalent to the HSD transport approach [23–25]. The implementation of the hadronic decays into dileptons (π-, η-, η'-, ω-, Δ-, a_1-Dalitz, $\rho \to l^+l^-$, $\omega \to l^+l^-$, and $\phi \to l^+l^-$) in HSD (and PHSD) is described in detail in Refs. [27] and [14]. For the treatment of the leptonic decays of open charm mesons and charmonia, we refer the reader to Refs. [10,17], and [18] for a detailed description.

The PHSD off-shell transport approach is particularly suitable for investigating the different scenarios for the modification of vector mesons in a hot and dense medium. Just as the HSD model, the PHSD approach incorporates the *off-shell propagation* for vector mesons as described

in Ref. [26]. In the off-shell transport, the hadron spectral functions change dynamically during the propagation through the medium and evolve toward the on-shell spectral functions in the vacuum. As demonstrated in Ref. [27], the off-shell dynamics is important for resonances with a rather long lifetime in the vacuum but strongly decreasing lifetime in the nuclear medium (especially ω and ϕ mesons), and also proves vital for the correct description of dilepton decays of ρ mesons with masses close to the two-pion decay threshold. For a detailed description of the off-shell dynamics and the implementation of vector-meson modifications in medium, we refer the reader to Refs. [14,26,27,32], and [11].

In Ref. [11], the extension of the hadronic sources in the PHSD for dilepton production to include secondary multiple-meson interactions by incorporating the channels $\pi\omega \to l^+l^-$, $\pi a_1 \to l^+l^-$, and $\rho\rho \to l^+l^-$ is described in detail. These so-called 4π channels for dilepton production are incorporated in the PHSD on a microscopic level, rather than assuming thermal dilepton production rates and incorporating a parametrization for the inverse reaction $\mu^+ + \mu^- \to 4\pi's$ by employing the detailed balance, as in Refs. [35] and [36]. By studying the electromagnetic emissivity (in the dilepton channel) of the hot hadron gas, it was shown in Refs. [37] and [38] that the dominating hadronic reactions contributing to the dilepton yield at the invariant masses above the ϕ peak are the two-body reactions of $\pi + \rho, \pi + \omega, \rho + \rho$, and $\pi + a_1$. This conclusion was supported by the subsequent study in a hadronic relativistic transport model [39]. Therefore, we have implemented the above-listed two-meson dilepton production channels in the PHSD approach. In addition, some higher vector mesons (ρ', etc.) are tacitly included by using phenomenological form factors that are adjusted to the experimental data (cf. Ref. [11]). Specifically, we determined the cross sections for the mesonic interactions with dileptons in the final state using an effective Lagrangian approach, following the works of Refs. [37] and [39]. In order to fix the form factors in the cross sections for dilepton production by the interactions of $\pi + \rho$, $\pi + \omega$, $\rho + \rho$ and πa_1, we used the measurements in the detailed-balance related channels: $e^+e^- \to \pi + \rho$, $e^+e^- \to \pi + \omega$, $e^+e^- \to \rho + \rho$, and $e^+e^- \to \pi + a_1$. Note that we fitted the form factors while taking into account the widths of the ρ and a_1 mesons in the final state by convoluting the cross sections with the (vacuum) spectral functions of these mesons in line with Ref. [40] (using the parametrizations of the spectral functions as implemented in the HSD and described in Ref. [41]). In Fig. 5 of Ref. [11] we have presented the resulting cross sections, which are implemented in the PHSD.

III. COMPARISON TO DATA

Let us first note that the bulk properties of heavy-ion collisions at the top RHIC energy, such as the number of charged particles as well as their rapidity, p_T, v_2, and transverse energy distributions, are rather well described by the PHSD; we refer to Ref. [22] for an extended and detailed comparison to the data from the PHOBOS, STAR, and PHENIX Collaborations. Since the lQCD equation of state employed in the PHSD has a crossover transition, the PHSD calculations show a rather long QGP phase in central Au + Au collisions at $\sqrt{s_{NN}} = 200$ GeV (cf. Fig. 6 of Ref. [22]) with the partonic degrees of freedom dominating for about 5–7 fm/c. We recall that dilepton production in the elementary pp channel is also well under control in the PHSD, as was previously demonstrated in Ref. [14].

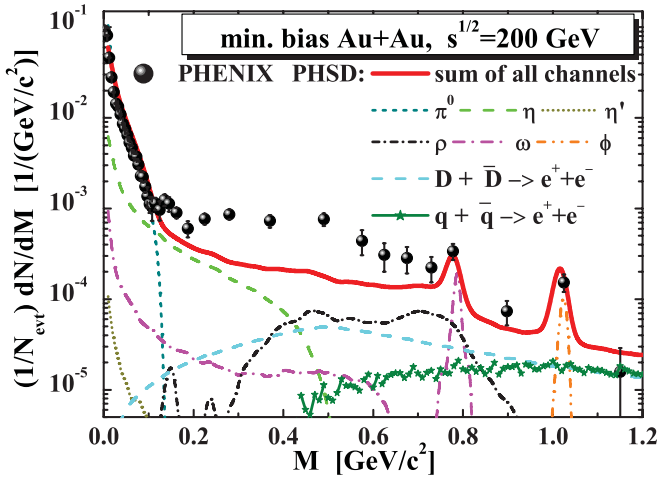

FIG. 1. (Color online) The PHSD results for the invariant mass spectra of inclusive dileptons in Au + Au collisions at $\sqrt{s_{NN}} = 200$ GeV within the PHENIX acceptance cuts, Eq. (1), in comparison to the data from the PHENIX Collaboration [7,8] for invariant masses $M = 0$–1.2 GeV. The different lines indicate the contributions from different channels as specified in the figure.

In Fig. 1 we show our results for the invariant mass spectra of inclusive dileptons in Au + Au collisions in the invariant mass region $M = 0$–1.2 GeV, for the acceptance cuts on single electron transverse momenta p_{eT}, pseudorapidities η_e, azimutal angle ϕ_e, and dilepton pair rapidity y:

$$\begin{gathered} p_{eT} > 0.2 \text{ GeV}, \\ |\eta_e| < 0.35, \\ -3\pi/16 < \phi_e < 5\pi/16, \ 11\pi/16 < \phi_e < 19\pi/16, \\ |y| < 0.35. \end{gathered} \tag{1}$$

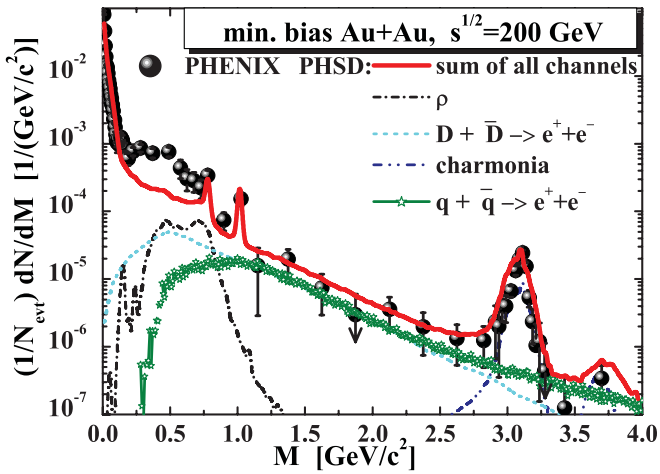

FIG. 2. (Color online) Same as Fig. 1 for invariant masses $M =$ 0–4 GeV.

In this region, the dilepton yield in the PHSD is dominated by hadronic sources and essentially coincides with the earlier HSD result [14]. There is a sizable discrepancy between the PHSD calculations and the data from the PHENIX Collaboration in the region of masses from 0.2 to 0.6 GeV. The discrepancy is not amended by the inclusion of the radiation from the QGP as well as from correlated D-meson decays, since the latter contributions are "overshone" by the radiation from hadrons integrated over the entire evolution of the collision.

In contrast, the partonic radiation as well as the yield from correlated D-meson decays are dominant in the mass region $M = 1$–4 GeV, as seen in Fig. 2, i.e., in the mass region between the ϕ and J/Ψ peaks. The dileptons generated by the quark-antiquark annihilation in the sQGP constitute about half of the observed yield in this intermediate-mass range. For $M >$ 2.5 GeV the partonic yield even dominates over the D-meson contribution. Thus, the inclusion of the partonic radiation in the PHSD fills up the gap between the hadronic model results [10,14] and the data of the PHENIX Collaboration for $M > 1$ GeV. Note that the collisional broadening scenario for the modification of the ρ meson was used in the calculations presented in Figs. 1 and 2.

A. Centrality dependence

Next we investigate the centrality dependence of dilepton production in heavy-ion collisions at the top RHIC energy for the centrality cuts specified in Eq. (1). While results from the PHSD calculations are in a reasonable agreement with the PHENIX data at 20%–40% centrality, the data show an increasing excess over the PHSD results for the 10%–20% centrality in the mass regime from 0.15 to 0.7 GeV, and this excess becomes even more dramatic for the most central (0%–10% centrality) collisions [cf. Figs. 3(a)–3(c)]. For all these centrality cuts, the contribution of partonic channels from the PHSD is subleading for $0.15 < M < 0.7$ GeV and cannot be responsible for the excess dileptons seen experimentally by the PHENIX Collaboration. In short, the early expectation of a partonic signal in the low-mass dilepton spectrum is not verified by the microscopic PHSD calculations.

B. Channel decomposition in central collisions

In order to elucidate the relative importance of the different *hadronic* sources of the excess dileptons in heavy-ion collisions at the top RHIC energy, we show in Fig. 4 the channel decomposition of the main hadronic contributions to

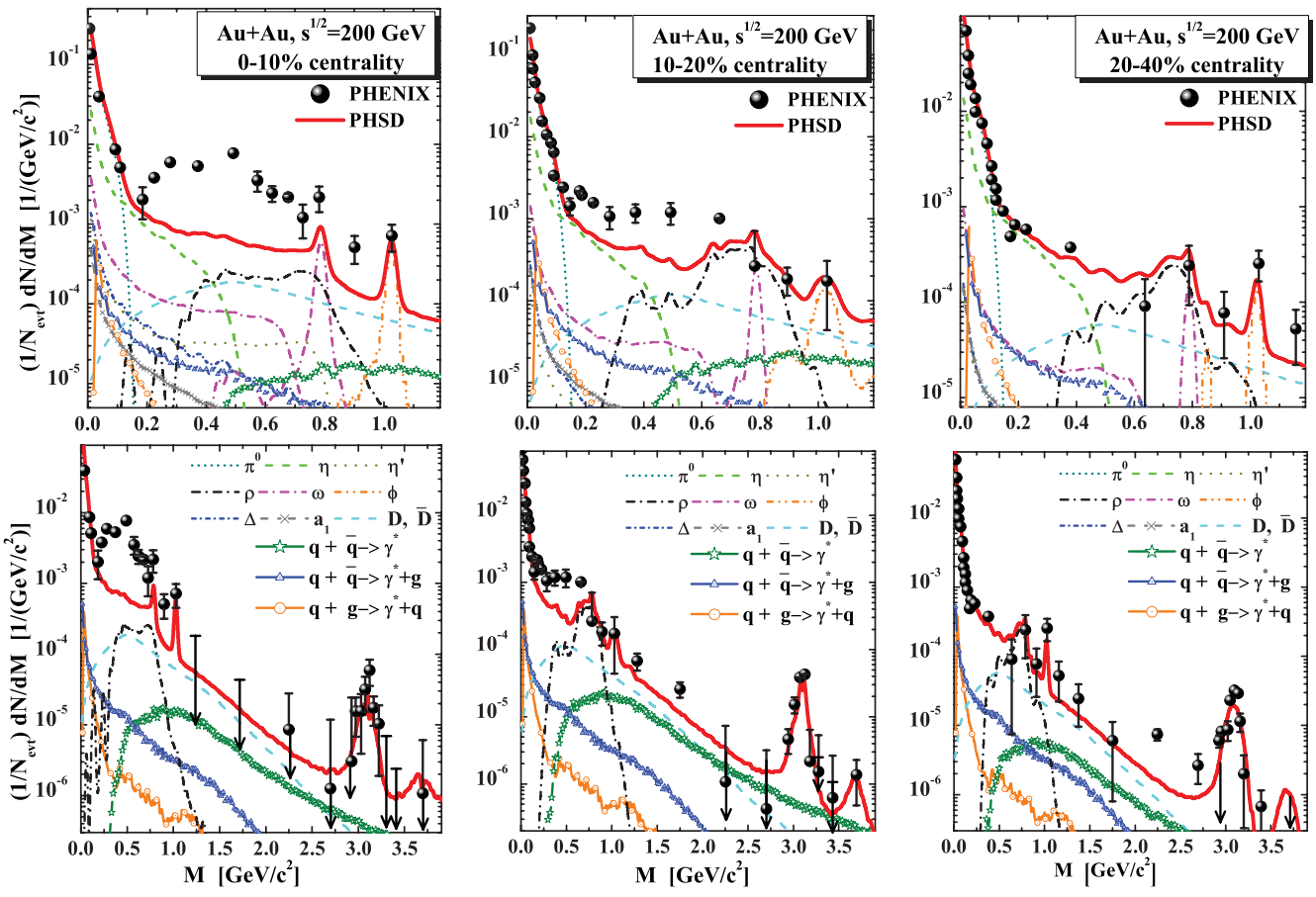

(a)0-10% centrality (b)10-20% centrality (c)20-40% centrality

FIG. 3. (Color online) The PHSD results for the dilepton invariant mass spectra in Au + Au collisions of different centralities at $\sqrt{s_{NN}} =$ 200 GeV in comparison to the data from the PHENIX Collaboration [7,8].

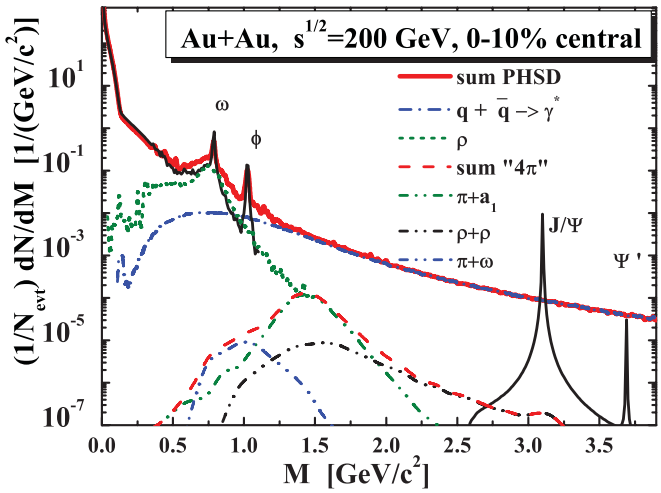

FIG. 4. (Color online) Dilepton invariant mass spectra from central Au + Au collisions at $\sqrt{s_{NN}} = 200$ GeV integrated over rapidity and transverse momenta as calculated in PHSD. The contributions from multiple-pion channels, quark-antiquark annihilation, and hadron decays into dileptons are shown separately.

the dilepton rates in central Au + Au collisions at $\sqrt{s_{NN}} =$ 200 GeV without any cuts on dilepton momenta and rapidity and without including the finite mass resolution of the PHENIX detector system. The blue (thin solid) line with its sharp peaks from the decay of vector mesons and a smooth background from the Dalitz decays of hadrons becomes rather insignificant above the ϕ-meson mass. Also the 4π channels ($\pi + a_1, \pi + \omega, \pi + \rho$, and $\rho + \rho$) are clearly subleading in the intermediate-mass region. Here the partonic channels—dominated by $q + \bar{q} \to e^+e^-$—constitute about half of the dilepton yield and have about the same contribution as that from correlated D-meson decays (not shown in Fig. 4). Note that the contribution from partonic channels is approximately exponential in mass for $1 < M < 2.5$ GeV, and might be interpreted as being due to "thermal radiation" from the sQGP. However, the PHSD calculations do not indicate that a thermal equilibrium has been achieved on the partonic level.

C. Transeverse momentum distributions

The PHENIX Collaboration has also accessed the information on the transverse momentum dependence of dilepton production by measuring the p_T spectra of dileptons in different bins of invariant mass M. In Fig. 5 we show the measured transverse momentum spectra of dileptons for minimum-bias Au + Au collisions at $\sqrt{s_{NN}} = 200$ GeV (symbols) in comparison with the spectra from the PHSD (lines) for six mass bins as indicated in the figure. Whereas the PHSD can well describe the dilepton spectra in the mass intervals [0, 100] and [810, 990] MeV, it underestimates the low-p_T dileptons in the other mass bins, particularly in the mass bin [300, 500] MeV. On the other hand, high-p_T dileptons are reproduced quite well by the PHSD calculations. We conclude that the missing dilepton yield for masses from 0.15 to 0.6 GeV is essentially due to a severe underestimation of the data at low p_T by up to an order of magnitude. We recall that at top SPS energies the low-p_T dilepton yield could be attributed

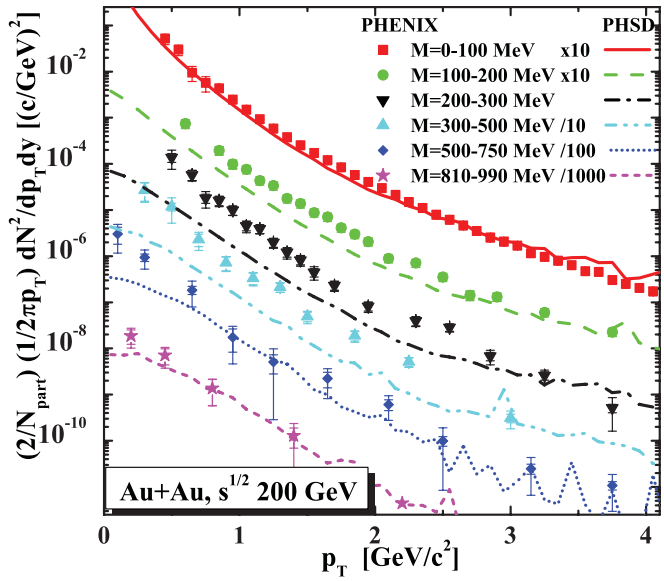

FIG. 5. (Color online) The PHSD results for the transverse-momentum spectra of dileptons from minimum bias Au + Au collisions at $\sqrt{s_{NN}} = 200$ GeV in different mass bins, compared to the data from the PHENIX Collaboration [7,8].

to π-π annihilation channels, i.e., to the soft hadronic reactions in the expansion phase of the system. These channels are, however, insufficient to describe the very low slope of the p_T spectra at the top RHIC energy.

D. Comparison with other models

Since the authors have worked on the topic of dilepton production within various approaches, it is instructive to discuss the results, especially in the low-mass regime for the same centralities and within the acceptance cuts in Eq. (1). In Fig. 6 we thus present the invariant mass spectra of

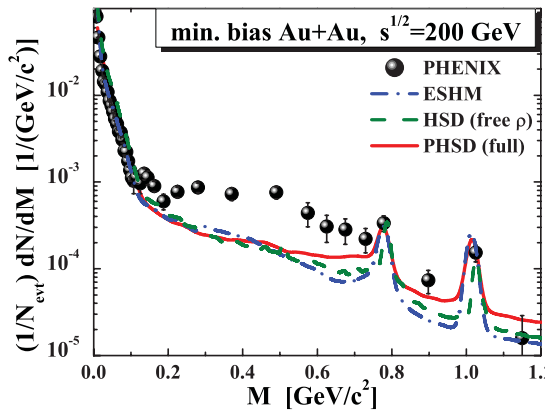

FIG. 6. (Color online) Invariant mass spectra of inclusive dileptons in Au + Au collisions at $\sqrt{s_{NN}} = 200$ GeV in the low-mass region ($M = 0$–1.2 GeV) as calculated in three models—PHSD taking into account in-medium modification of ρ mesons and dilepton radiation from the partonic phase (solid line); HSD in the free-ρ scenario (dashed line); and the extended thermal model [10]—compared to the data from the PHENIX Collaboration [7,8].

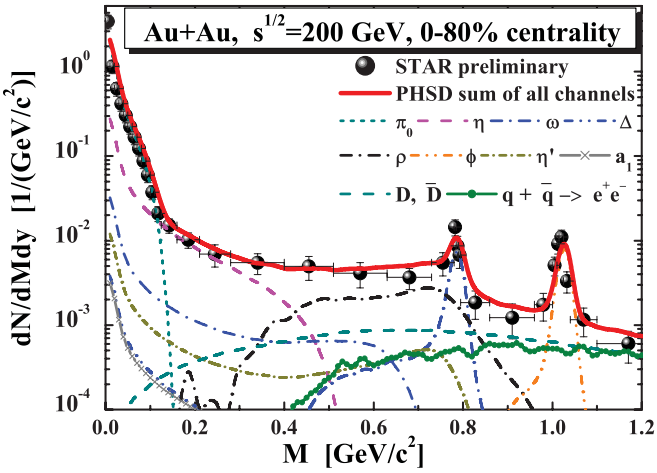

FIG. 7. (Color online) The PHSD results for the invariant mass spectra of inclusive dileptons in Au + Au collisions at $\sqrt{s_{NN}} =$ 200 GeV for $M = 0$–1.2 GeV and 0%–80% centrality within the cuts of the STAR experiment; see Eq. (2). The preliminary data from the STAR Collaboration are adopted from Ref. [60].

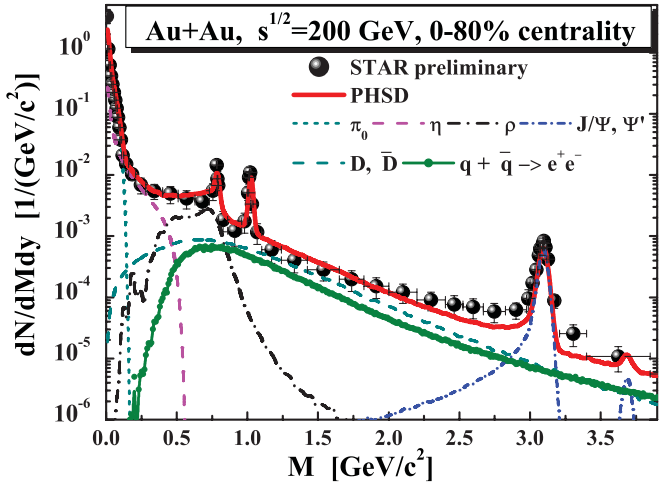

FIG. 8. (Color online) Same as Fig. 7 for $M = 0$–4 GeV.

inclusive dileptons in Au + Au collisions at $\sqrt{s_{NN}} = 200$ GeV in the low-mass region ($M = 0$–1.2 GeV) as calculated within (1) PHSD (red solid line) taking into account the in-medium modification of the ρ as well as the dilepton radiation from the partonic phase; (2) HSD in the free-ρ scenario; and (3) the extended statistical hadronization model [10] in comparison to the data from the PHENIX Collaboration [7,8].

The extended statistical hadronization model (ESHM) [10] is an extension to the statistical hadronization model (SHM) which has been applied [42–55] to high-energy elementary and especially heavy-ion collision experiments in order to calculate the yields of different hadron species. In the SHM, the state of the "thermal" fireball is specified by its temperature T, volume V, and the chemical potentials μ_B, μ_Q, and μ_S for baryon, electric, and strangeness charges, respectively. While μ_S and μ_Q are zero in central Au + Au collisions at $\sqrt{s_{NN}} =$ 200 GeV, μ_B is about 30 MeV. The effect of the strangeness undersaturation parameter or fugacity γ_S on the dielectron invariant mass spectrum as a function of centrality was studied in detail in Ref. [10], and the effect was found to be moderate. We employ the value $\gamma_S = 0.6$ in this work for the minimum-bias Au + Au collisions. The overall normalization (fireball volume) at different centralities was fitted to experimental data in Ref. [10], and we use the same values throughout. For the temperature we use the value $T = 170$ MeV.

Since the measured rapidity and transverse momentum spectra of hadrons emitted in the high-energy collision experiments do not resemble thermal distributions, the SHM has been extended in Ref. [10] by boosting (event by event) the "fireball" along the beam axis so that the rapidity distributions of pions become compatible with the BRAHMS measurements [56]. Also, the problem that the SHM tends to overpopulate the low-p_T part of the spectrum compared with the experimental distributions was solved in the ESHM by assuming that the created clusters' transverse momentum is normally distributed with the width fitted together with the system volume V to the PHENIX data [57] in $p + p$ collisions and in 11 different centrality classes in the case of Au+Au collisions. For further details we refer the reader to Ref. [10].

We find in Fig. 6 that the HSD and the ESHM give approximately the same results on the level of 30% for the dilepton invariant mass spectra. This might be surprising since the HSD includes not only the direct and Dalitz decays of hadrons but also meson-meson and meson-baryon channels for dileptons. Indeed, the enhancement of the HSD result from 0.55 to 0.75 GeV can be traced back to pion-pion annihilation which, however, gives only a small contribution at the top RHIC energy. Our actual PHSD calculations show some more dilepton yield in the ρ-mass regime as a result of the broadened ρ spectral function employed in the calculations. In the free-ρ scenario, the results from HSD and PHSD are identical within statistics, since the partonic channels give only a small contribution in this mass range. The conclusion that the dilepton spectrum at masses below 1 GeV is dominated by the hadronic sources is also supported by the studies in other available models [58,59].

E. Predictions for STAR and comparison to preliminary data

The PHSD calculations allow us to match with the different experimental conditions and thus to provide a theoretical link between the different measurements. To this extent, we have provided the differential data tables for our theoretical predictions on our web site [61] so that any acceptance cuts and experimental mass and transverse momentum resolutions can be applied.

The STAR Collaboration at RHIC has recently measured dileptons from Au + Au collisions at $\sqrt{s_{NN}} = 200$ GeV with the acceptance following cuts on single electron transverse momenta p_{eT}, single electron pseudorapidities η_e, and the dilepton pair rapidity y:

$$0.2 < p_{eT} < 5 \text{ GeV}, \quad |\eta_e| < 1, \quad |y| < 1. \tag{2}$$

Our predictions for the dilepton yield within these cuts are shown in Figs. 7 and 8 for 0%–80% centrality and in Figs. 9 and 10 for 0%–10% centrality. One can observe generally a

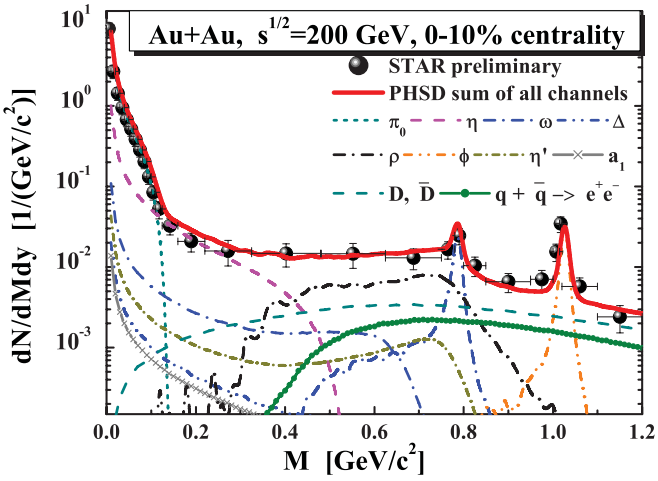

FIG. 9. (Color online) The PHSD results for the invariant mass spectra of inclusive dileptons in Au + Au collisions at $\sqrt{s_{NN}} =$ 200 GeV for $M = 0$–1.2 GeV and 0%–80% centrality within the cuts of the STAR experiment; see Eq. (2). The preliminary data from the STAR Collaboration are adopted from Ref. [60].

good agreement with the preliminary data from the STAR Collaboration [60] for 0%–80% centrality in the whole mass regime. Surprisingly, our calculations are also roughly in line with the low-mass dilepton spectrum from STAR [60] in the case of central collisions, whereas the PHSD results severely underestimate the PHENIX data for the cuts given in Eq. (1) (cf. Fig. 3). The observed yield from STAR can be accounted for by the known hadronic sources, i.e., the decays of the π_0, η, η', ω, ρ, ϕ, and a_1 mesons, of the Δ particle, and the semileptonic decays of the D and $\bar{D}$ mesons, where the collisional broadening of the ρ meson is taken into account. At first sight this observation might point toward an inconsistency between the data sets from PHENIX and STAR, but we have to stress that the actual experimental acceptance cuts are more sophisticated than those given in Eqs. (1) and (2). This problem will have to be investigated more closely by the experimental collaborations. Furthermore, the upgrade of the PHENIX

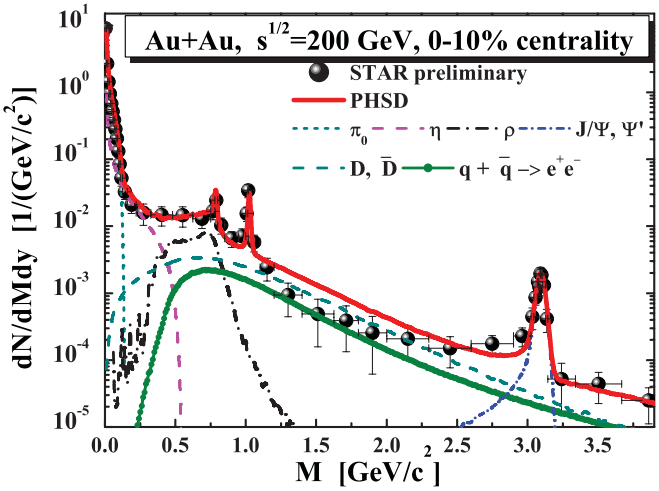

FIG. 10. (Color online) Same as Fig. 9 for $M = 0$–4 GeV.

experiment with a hadron blind detector [62] should provide decisive information on the origin of the low-mass dileptons produced in the heavy-ion collisions at $\sqrt{s} = 200$ GeV.

We also observe a slight overestimation of the dilepton yield from PHSD in 0%–10% central collisions at masses from 1.3 to 1.8 GeV, where the dominant contributions to the spectrum are the radiation from the sQGP and the semileptonic decays of the D and $\bar{D}$ mesons. We speculate that the suppression of dileptons from the D and $\bar{D}$ mesons might be underestimated in the PHSD calculations in central collisions. The upgrade of the STAR detector [63] will be promising in independently measuring the correlated D and $\bar{D}$ meson contributions.

IV. SUMMARY

In this study, we have addressed dilepton production in Au + Au collisions at $\sqrt{s_{NN}} = 200$ GeV by employing the parton-hadron-string dynamics (PHSD) off-shell transport approach. This work is a continuation of our earlier studies for heavy-ion collisions at the SIS energies of 1–2 A GeV [27] and the SPS energies from 40 to 158 A GeV [11,14], essentially within the same dynamical transport model. Within the PHSD one solves generalized transport equations on the basis of the off-shell Kadanoff-Baym equations for effective Green's functions in phase-space representation (beyond the quasiparticle approximation) for quarks, antiquarks and gluons as well as for the hadrons and their excited states. The PHSD approach consistently describes the full evolution of a relativistic heavy-ion collision, from the initial hard scatterings and string formation, through the dynamical deconfinement phase transition to the quark-gluon plasma (QGP) as well as hadronization, to the subsequent interactions in the hadronic phase. It was shown in previous studies that the PHSD approach well describes the various hadron abundancies, their longitudinal rapidity distributions, as well as transverse momentum distributions from lower SPS to top RHIC energies [21,22]. Also, the collective flow $v_2(p_t)$ is roughly in accordance with the experimental observations by the PHOBOS, STAR, and PHENIX Collaborations at RHIC [22]. The latter findings allow us explore the dynamics of subleading or rare probes within the dynamical environment of partons and hadrons during the complex time evolution of a relativistic heavy-ion collision.

The present study has been devoted particularly to the calculation of dilepton radiation from partonic interactions through the reactions $q\bar{q} \to \gamma^*$, $q\bar{q} \to \gamma^* + g$, and $qg \to \gamma^* q$ ($\bar{q}g \to \gamma^* \bar{q}$) in the early stage of relativistic heavy-ion collisions at the top RHIC energy. We recall that the differential cross sections for electromagnetic radiation have been calculated with the same propagators as those incorporated in the PHSD transport approach. By comparing our calculated results to the data from the PHENIX Collaboration, we have studied the relative importance of different dilepton production mechanisms and addressed in particular the "PHENIX puzzle" of a large enhancement of dileptons in the mass range from 0.15 to 0.6 GeV as compared to the emission of hadronic states. Our studies have demonstrated that the observed excess in the low-mass dilepton regime cannot be attributed to partonic productions as expected earlier. Thus the PHENIX puzzle

still has no explanation from the theoretical approaches so far. The PHENIX enhancement is essentially due to dileptons of low transverse momentum in the mass range from 0.15 to 0.6 GeV, and to date finds no explanation by hadronic or partonic reaction channels in PHSD that occur on top of the interactions in pp collisions during the evolution of relativistic heavy-ion collisions.

Similar to our findings at SPS energies [11], we find that the partonic dilepton production channels are visible in the intermediate-mass region between the ϕ and J/Ψ peaks. Their contribution is about as large as the correlated background from D-meson decays. Surprisingly, this contribution appears to be exponential in mass from 1 to 2.5 GeV so that an appropriate interpretation might appear to be thermal radiation from the sQGP. However, the PHSD dynamics shows that no kinetic equilibrium is achieved on the partonic level in heavy-ion collisions at top RHIC energies, and such an interpretation has to be considered with care.

In view of the fact that within different (statistical and dynamical) models we have not been able to find an explanation for the low-mass PHENIX puzzle, the solution has to be relegated to the experimental side. In fact, the STAR Collaboration has taken independent dilepton data for centralities different from the PHENIX measurements and also with different detector acceptances. Our PHSD calculations allow us to match with the different experimental conditions and thus to provide a theoretical link between the different measurements. To this extent, we have provided our predictions [61] for the conditions of the STAR experiment, which happen to be in a rough agreement with the preliminary data from the STAR Collaboration [60]. This finding opens up new challenges that will have to be addressed from the experimental side. The upgrade of the PHENIX experiment with a hadron blind detector [62] and the upgrade of the STAR detector [63] for independently measuring the correlated D and $\bar{D}$ meson contributions appear mandatory to shed some further light on the present "puzzles".

ACKNOWLEDGMENTS

The authors are grateful for fruitful discussions with X. Dong, T. Hemmick, B. Jacak, L. Ruan, I. Tserruya, A. Toia, and N. Xu. They also acknowledge financial support through the "HIC for FAIR" framework of the LOEWE program and the Deutsche Forschungsgemeinschaft (DFG). The work of C.M.K was supported by the US National Science Foundation under Grants No. PHY-0758115 and No. PHY-1068572, the US Department of Energy under Contract No. DE-FG02-10ER41682, and the Welch Foundation under Grant No. A-1358.

[1] E. V. Shuryak, Sov. Phys. JETP **47**, 212 (1978).
[2] E. V. Shuryak, Phys. Lett. B **78**, 150 (1978); Sov. J. Nucl. Phys. **28**, 408 (1978); Yad. Fiz. **28**, 796 (1978).
[3] E. L. Feinberg, Izv. Akad. Nauk Ser. Fiz. **34**, 1987 (1970).
[4] E. L. Feinberg, Nuovo Cimento A **34**, 391 (1976).
[5] J. D. Bjorken and H. Weisberg, Phys. Rev. D **13**, 1405 (1976).
[6] A. Adare *et al*., Phys. Lett. B **670**, 313 (2009).
[7] A. Toia *et al*., Nucl. Phys. A **774**, 743 (2006); Eur. Phys. J **49**, 243 (2007); S. Afanasiev *et al*., e-print arXiv:0706.3034.
[8] A. Adare *et al*., Phys. Rev. C **81**, 034911 (2010).
[9] O. Linnyk, E. L. Bratkovskaya, and W. Cassing, AIP Conf. Proc. **1257**, 700 (2010).
[10] J. Manninen, E. L. Bratkovskaya, W. Cassing, and O. Linnyk, Eur. Phys. J. C **71**, 1615 (2011).
[11] O. Linnyk, E. L. Bratkovskaya, V. Ozvenchuk, W. Cassing, and C. M. Ko, Phys. Rev. C **84**, 054917 (2011).
[12] R. Arnaldi *et al*., Phys. Rev. Lett. **96**, 162302 (2006); J. Seixas *et al*., J. Phys. G **34**, S1023 (2007); S. Damjanovic *et al*., Nucl. Phys. A **783**, 327c (2007); R. Arnaldi *et al*., Eur. Phys. J. C **61**, 711 (2009).
[13] R. Arnaldi *et al*. (NA60 Collaboration), Eur. Phys. C **59**, 607 (2009).
[14] E. L. Bratkovskaya, W. Cassing, and O. Linnyk, Phys. Lett. B **670**, 428 (2009).
[15] K. Dusling, D. Teaney, and I. Zahed, Phys. Rev. C **75**, 024908 (2007); K. Dusling and I. Zahed, *ibid*. **80**, 014902 (2009); Nucl. Phys. A **825**, 212 (2009).
[16] A. Toia, J. Phys. G **35**, 104037 (2008).
[17] O. Linnyk, E. L. Bratkovskaya, and W. Cassing, Int. J. Mod. Phys. E **17**, 1367 (2008).
[18] O. Linnyk, E. L. Bratkovskaya, W. Cassing, and H. Stöcker, Phys. Rev. C **76**, 041901 (2007).
[19] K. Gallmeister, B. Kämpfer, and O. P. Pavlenko, Phys. Lett. B **473**, 20 (2000).
[20] K. Gallmeister, B. Kämpfer, O. P. Pavlenko, and C. Gale, Nucl. Phys. A **688**, 939 (2001).
[21] W. Cassing and E. L. Bratkovskaya, Nucl. Phys. A **831**, 215 (2009).
[22] E. L. Bratkovskaya, W. Cassing, V. P. Konchakovski, and O. Linnyk, Nucl. Phys. A **856**, 162 (2011).
[23] W. Cassing and E. L. Bratkovskaya, Phys. Rep. **308**, 65 (1999).
[24] E. L. Bratkovskaya and W. Cassing, Nucl. Phys. A **619**, 413 (1997).
[25] W. Ehehalt and W. Cassing, Nucl. Phys. A **602**, 449 (1996).
[26] W. Cassing and S. Juchem, Nucl. Phys. A **665**, 377 (2000); **672**, 417 (2000).
[27] E. L. Bratkovskaya and W. Cassing, Nucl. Phys. A **807**, 214 (2008).
[28] W. Cassing and E. L. Bratkovskaya, Phys. Rev. C **78**, 034919 (2008).
[29] W. Cassing, Eur. Phys. J. ST **168**, 3 (2009).
[30] A. Peshier, B. Kämpfer, O. P. Pavlenko, and G. Soff, Phys. Rev. D **54**, 2399 (1996); P. Levai and U. Heinz, Phys. Rev. C **57**, 1879 (1998); A. Peshier, B. Kämpfer, and G. Soff, *ibid*. **61**, 045203 (2000); Phys. Rev. D **66**, 094003 (2002); M. Bluhm, B. Kampfer, R. Schulze, D. Seipt, and U. Heinz, Phys. Rev. C **76**, 034901 (2007).
[31] A. Peshier and W. Cassing, Phys. Rev. Lett. **94**, 172301 (2005).
[32] O. Linnyk, E. L. Bratkovskaya, J. Manninen, and W. Cassing, J. Phys. Conf. Ser. **312**, 012010 (2011).
[33] O. Linnyk, S. Leupold, and U. Mosel, Phys. Rev. D **71**, 034009 (2005).
[34] O. Linnyk, J. Phys. G **38**, 025105 (2011).
[35] H. van Hees and R. Rapp, Nucl. Phys. A **806**, 339 (2008).

[36] E. Santini, J. Steinheimer, M. Bleicher, and S. Schramm, Phys. Rev. C **84**, 014901 (2011).
[37] C. Song, C. M. Ko, and C. Gale, Phys. Rev. D **50**, 1827 (1994).
[38] C. Gale and P. Lichard, Phys. Rev. D **49**, 3338 (1994).
[39] G.-Q. Li and C. Gale, Phys. Rev. C **58**, 2914 (1998).
[40] C. Song and C. M. Ko, Phys. Rev. C **53**, 2371 (1996).
[41] E. L. Bratkovskaya, S. M. Kiselev, and G. B. Sharkov, Phys. Rev. C **78**, 034905 (2008).
[42] I. Kraus, J. Cleymans, H. Oeschler, K. Redlich, and S. Wheaton, Phys. Rev. C **76**, 064903 (2007).
[43] F. Becattini, P. Castorina, J. Manninen, and H. Satz, Eur. Phys. J. C **56**, 493 (2008).
[44] A. Andronic, F. Beutler, P. Braun-Munzinger, K. Redlich, and J. Stachel, Phys. Lett. B **678**, 350 (2009).
[45] F. Becattini, J. Cleymans, A. Keränen, E. Suhonen, and K. Redlich, Phys. Rev. C **64**, 024901 (2001).
[46] J. Cleymans, B. Kämpfer, and S. Wheaton, Phys. Rev. C **65**, 027901 (2002).
[47] A. Baran, W. Broniowski, and W. Florkowski, Acta Phys. Pol. B **35**, 779 (2004).
[48] J. Cleymans, B. Kämpfer, M. Kaneta, S. Wheaton, and N. Xu, Phys. Rev. C **71**, 054901 (2005).
[49] J. Rafelski, J. Letessier, and G. Torrieri, Phys. Rev. C **72**, 024905 (2005).
[50] A. Andronic, P. Braun-Munzinger, and J. Stachel, Nucl. Phys. A **772**, 167 (2006).
[51] F. Becattini, J. Manninen, and M. Gazdzicki, Phys. Rev. C **73**, 044905 (2006).
[52] J. Letessier and J. Rafelski, Eur. Phys. J. A **35**, 221 (2008).
[53] J. Manninen and F. Becattini, Phys. Rev. C **78**, 054901 (2008).
[54] A. Andronic, P. Braun-Munzinger, and J. Stachel, Phys. Lett. B **673**, 142 (2009); **678**, 516(E) (2009).
[55] J. Noronha-Hostler, J. Noronha, and C. Greiner, J. Phys. G **37**, 094062 (2010).
[56] I. G. Bearden *et al*., Phys. Rev. Lett. **94**, 162301 (2005).
[57] S. S. Adler *et al*., Phys. Rev. C **74**, 024904 (2006); **69**, 034909 (2004).
[58] R. Rapp, AIP Conf. Proc. **1322**, 55 (2010).
[59] Y. Akamatsu, H. Hamagaki, T. Hatsuda, and T. Hirano, e-print arXiv:1107.3612.
[60] STAR, J. Zhao, J. Phys. G **38**, 124134 (2011).
[61] The PHSD predictions presented in Figs. 7–10 can be downloaded from the web page [http://fias.uni-frankfurt.de/∼linnyk/RHICdil/].
[62] W. Anderson *et al*., Nucl. Instrum. Methods Phys. Res. A **646**, 35 (2011).
[63] L. Ruan *et al*., J. Phys. G **36**, 095001 (2009).